magnetism

MDPI

Article

Magnetoelastic Resonance Sensing for Structural Health Monitoring of Cementitious Materials

Georgios Samourgkanidis

Department of Civil and Environmental Engineering, University of Cyprus, 1678 Nicosia, Cyprus; samourgkanidis.georgios@ucy.ac.cy

Abstract

This study investigates the use of magnetoelastic sensing for vibration-based structural health monitoring (SHM) of cementitious beam specimens under intact and damaged conditions. Prismatic mortar beams with dimensions of $160 \times 40 \times 40$ mm^3 were fabricated following standardized preparation procedures and equipped with annealed amorphous ferromagnetic ribbons, Metglas 2826MB3, for nondestructive magnetoelastic vibration sensing. The specimens were tested under free-vibration conditions in a simply supported configuration, and their vibration response was measured using a detection coil and subsequently analyzed using MATLAB software. The undamaged specimen exhibited a dominant resonance frequency at 6531 Hz, which closely corresponded to the fourth bending mode predicted by Euler–Bernoulli beam theory. Controlled notch-shaped cracks with varying locations and depths were subsequently introduced to evaluate the sensitivity of the sensing system to structural damage. Experimental results showed that the frequency shift is strongly influenced by the location of damage relative to the modal nodes, with maximum sensitivity observed between nodal regions and minimal variation near the nodes. Furthermore, increasing notch-shaped crack depth produced progressively larger frequency shifts, revealing a monotonic and non-linear relationship between damage severity and dynamic response. Polynomial fitting and 3D surface analysis further highlighted the combined influence of crack location and depth on the measured frequency variation. The findings confirm that the magnetoelastic sensor is capable of accurately detecting and magnetically transmitting the vibration state and damage-induced changes in cementitious structures, demonstrating high sensitivity and strong potential for application in vibration-based structural health monitoring systems, particularly in materials characterized by strong vibration damping.

Keywords: structural health monitoring; resonance frequency shift; magnetoelastic sensors; smart sensing materials; electromagnetic sensing

Check for updates

Academic Editor: Qifan Li

Received: 28 May 2026
Revised: 23 June 2026
Accepted: 26 June 2026
Published: 30 June 2026

Copyright: © 2026 by the author. Licensee MDPI, Basel, Switzerland. This article is an open access article distributed under the terms and conditions of the Creative Commons Attribution (CC BY) license.

1. Introduction

The continuous assessment of civil infrastructure has become increasingly important due to the aging of structural systems and the growing demand for safety, reliability, and serviceability in modern society. To address these challenges, a wide range of structural health monitoring (SHM) techniques has been developed over the past few decades, aiming to detect, locate, and quantify damage in engineering structures [1]. These techniques generally include visual inspection, localized non-destructive testing methods, and global monitoring approaches based on structural response measurements. While traditional

inspection methods remain widely used in practice, they are often limited by their dependence on human evaluation and their inability to provide continuous or real-time information about structural condition. As a result, research has progressively shifted toward sensor-based monitoring systems capable of capturing the evolving behavior of structures under operational conditions.

Among modern SHM approaches, sensor-based technologies have emerged as one of the most effective solutions for continuous and real-time monitoring of structural conditions [2–4]. Various sensing systems have been proposed for civil engineering applications, including strain gauges [5–9], piezoelectric transducers [10–14], fiber optic sensors [15–19], accelerometers [20–24], acoustic emission sensors [25–29], laser Doppler vibrometers [30–34], and wireless sensing networks [35–39]. These technologies enable the measurement of different physical parameters, such as strain, acceleration, displacement, surface velocity, temperature, and wave propagation characteristics, providing valuable information regarding the integrity and performance of structural systems. The rapid development of smart sensing materials and advanced data acquisition techniques has further expanded the capabilities of SHM systems, allowing for improved sensitivity, automated monitoring, and integration with digital signal processing methods. In recent years, artificial intelligence (AI) and machine learning algorithms have also been increasingly incorporated into SHM frameworks, enabling automated pattern recognition, damage classification, anomaly detection, and predictive assessment of structural behavior from large volumes of sensor data [40,41]. Nevertheless, despite the significant progress achieved in sensor-based SHM systems, many conventional sensing technologies still encounter limitations associated with durability, installation complexity, power requirements, high equipment cost, and long-term operation under harsh environmental conditions, particularly in cementitious and large-scale civil infrastructure applications. These challenges have motivated growing interest in alternative sensing approaches based on smart functional materials capable of providing reliable and passive monitoring capabilities.

In this context, magnetic materials have attracted considerable attention due to their ability to interact with mechanical stimuli through electromagnetic phenomena, opening new possibilities for contactless SHM [42–44]. Magnetic-based sensing approaches have been investigated for monitoring stress, strain, crack formation, corrosion, and dynamic structural response in a variety of engineering materials [45–47]. Compared with traditional wired sensing systems, magnetic sensing techniques offer several potential advantages, including electromagnetic signal transmission, reduced dependence on direct electrical connections, high sensitivity to mechanical disturbances, and suitability for embedded or difficult-to-access structural regions. Within this broader category, magnetoelastic materials have emerged as particularly promising sensing elements [48,49] because of their ability to directly couple mechanical deformation with variations in magnetic flux. When subjected to mechanical stress or vibration, these materials experience changes in magnetization through the magnetoelastic effect, generating measurable magnetic signals that can be detected remotely using external pickup coils [50]. This sensing mechanism enables the monitoring of structural vibrations and damage-related changes without requiring complex instrumentation or continuous power supply at the sensing location [51].

Building on these characteristics, magnetoelastic sensing can be naturally extended from static or quasi-static monitoring applications toward dynamic, vibration-based SHM. Vibration-based SHM represents one of the most widely adopted global approaches for assessing the condition of engineering structures [52–54]. Its fundamental principle is based on the fact that damage within a structural system induces variations in mass, stiffness, and energy dissipation properties, which in turn alter its dynamic response. These changes are commonly observed through shifts in modal characteristics such as natural frequencies [55–57], mode shapes [58–60], and damping ratios [61–63], which serve as key indicators of structural

integrity. Within this framework, the effectiveness of vibration-based SHM systems is strongly dependent on the performance of the sensing technology, particularly in terms of sensitivity, stability, and long-term operability under field conditions. The structural response is therefore interpreted through its inherent dynamic properties, where damage-induced modifications in stiffness and boundary conditions are reflected as measurable changes in vibration behavior. In this context, magnetoelastic materials offer a promising sensing alternative by exploiting their stress-dependent magnetic response to directly transduce mechanical vibrations into remotely detectable electromagnetic signals [64]. This mechanism preserves information related to the underlying modal characteristics of the structure in the measured output signal. Consequently, magnetoelastic sensing establishes a direct link between material-level electromechanical coupling and global structural dynamics, providing a robust foundation for resonance-based condition assessment and damage identification in civil engineering systems.

2. Materials and Methods

The experimental specimens consisted of prismatic cementitious beams designed to investigate the vibration response under both intact and damaged conditions. All samples were fabricated in a controlled laboratory environment using commercially available materials to ensure repeatability and compliance with standardized mortar preparation procedures (Figure 1). The cementitious mixture was composed of Portland cement (Aspropyrgos, Attica, Greece), standard siliceous sand with a high silica content, and tap water. The mix proportions were maintained at a cement-to-sand mass ratio of 1:3, in accordance with the EN 196-1 standard [65] guidelines for cement mortar specimen preparation and the workability of the fresh mortar was adjusted to achieve a flow value of 165 ± 3 mm, as determined using the flow table test in accordance with EN 1015-3 [66]. The molding procedure was carried out in accordance with EN 196-1 by casting the mortar into prismatic specimens with dimensions of 160 × 40 × 40 mm^3, which were demolded after 24 h and subsequently cured in a water tank at 21 °C for 28 days prior to testing.



(**a**) (**b**) (**c**)

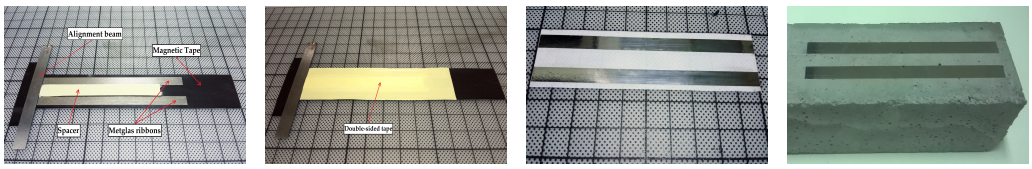
Figure 1. (**a**) Mechanical mixing of the cementitious mortar; (**b**) prepared steel molds prior to casting; and (**c**) demolded prismatic specimens ready for curing.

The next stage of the experimental procedure involved the preparation and attachment of the magnetoelastic sensors onto the cementitious specimens. In this study, amorphous ferromagnetic metallic alloy ribbons, commercially known as Metglas 2826MB3 (Table 1) and manufactured by Metglas Inc. (Conway, SC, USA), were employed. Prior to their installation on the cementitious beams, the ribbons were subjected to an annealing process aimed at enhancing their magnetic signal and improving their sensing response [67,68]. The attachment of the magnetoelastic ribbons to the cementitious specimens was carried out through a controlled multistep procedure to ensure accurate alignment and reliable bonding (Figure 2). Initially, a dedicated alignment setup, consisting of an alignment beam, a spacer, and a magnetic tape, was used to position two ribbons (dimensions

100 mm × 6 mm × 25 µm) in parallel configuration and at a predefined separation distance. The alignment beam and spacer ensured geometric consistency, while the magnetic tape provided temporary fixation to facilitate handling during the alignment process. Subsequently, a section of double-sided adhesive tape was carefully applied over the aligned ribbons and left in place for a few seconds to ensure adequate adhesion. The tape was then gently removed in such a way that both ribbons remained attached to its adhesive surface. In the final step, the tape carrying the two pre-aligned ribbons was mounted onto the cementitious specimen, ensuring that the ribbons were oriented parallel to the longitudinal axis of the specimen. Any excess adhesive tape was carefully trimmed using a rigid plastic blade to avoid surface damage to the beam and to ensure a clean and stable installation. The main reason for placing the Metglas ribbons parallel to the length of the specimen was to ensure proper fitting on the specimen surface. The selection of two 10 cm ribbons was based on findings from a previous study [69], where this configuration was sufficient to reliably capture the vibration behavior of the specimens.

Table 1. Physical and geometrical properties of Metglas 2826MB3 ribbons.

No.	Property	Metglas 2826MB3
1	Length	100 mm
2	Width	6 mm
3	Thickness	29 µm
4	Density	7.90 g/cm^{-3}
5	Modulus of elasticity	100–110 GPa
6	Stoichiometry	$Fe_{37}Ni_{42}Mo_4B_{17}$
7	Curie temperature	353 °C
8	Saturation induction	0.88 T
9	Saturation magnetostriction λ_s	12 ppm



(**a**) (**b**) (**c**) (**d**)

Figure 2. (**a**) Ribbon alignment setup; (**b**) application of double-sided adhesive tape over the ribbons; (**c**) two pre-aligned ribbons prepared for attachment to the cementitious specimen; and (**d**) Metglas ribbons attached at the cementitious specimen.

The sensing procedure was conducted in near room temperature conditions (22 °C) using a dedicated experimental setup, schematically presented in Figure 3.

A simply supported configuration was employed to define the boundary conditions of the cementitious specimens. Each specimen was placed on two metallic supports located at its edges and subjected to vibrational excitation [70]. Two different excitation procedures were conducted. Initially, each specimen was mechanically excited prior to the attachment of the Metglas ribbons, and the vibration response was measured without recording any signal. Subsequently, the same excitation procedure was repeated after attaching the ribbons to the specimens. This approach was adopted to verify that the recorded signals originated exclusively from the magnetoelastic sensors and to ensure that no parasitic noise or external interference affected the measurements. The excitation was achieved by dropping a metallic cone from a predetermined height using a specially designed setup, thereby inducing free vibration of the specimen. The cone setup shown in Figure 3 represents a simplified schematic of the actual configuration. In the real experimental

arrangement, the cone was mounted on a spring that enabled its retraction after impact. The drop height was selected such that, upon reaching the specimen surface, the spring was already slightly extended beyond its equilibrium position, ensuring near-maximum impact energy while still allowing post-impact retraction.

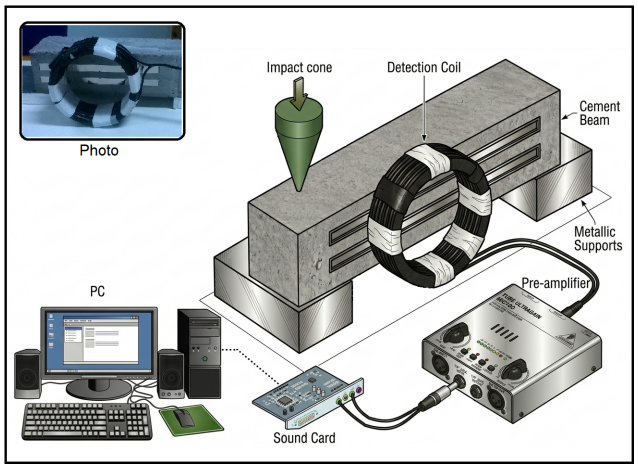


Figure 3. Schematic representation of the experimental setup used in the present study.

To ensure consistency and repeatability of the measurements, the excitation and recording procedures were repeated multiple times during the experiment (9 in total): 3 impacts were found at one simply supported end, 3 at the midpoint, and 3 at the other simply supported end. The final response was obtained by averaging the recorded signals over multiple excitation cycles. The signal recording was performed using a detection coil (Table 2) positioned close to the specimen and the attached Metglas ribbons. The detected signal was subsequently amplified using a pre-amplifier connected to the sound card of a PC, while all signal acquisition and processing procedures were carried out using MATLAB R2021b software. The recording of the signal from the Metglas ribbons is based on electromagnetic induction. When the cementitious specimen undergoes mechanical vibration, the attached Metglas ribbon experiences alternating mechanical stress due to the deformation of the material. Owing to the magnetoelastic effect, these stress variations induce continuous changes in the ribbon's magnetization, generating a varying magnetic flux around the ribbon. The nearby pickup coil detects these magnetic flux variations and converts them into an induced electrical voltage signal. The resulting voltage signal contains the vibration characteristics of the cementitious specimen, enabling the monitoring and analysis of its dynamic behavior, natural frequencies, and structural changes such as damage or cracking. In this work, damage was represented by a notch-shaped crack introduced transversely across the length of the specimen using a sawing machine. The notch had a constant width of 1 mm, while its depth varied from 1 to 5 mm, corresponding to 2.5% to 12.5% of the total height of the prismatic specimens, which was 40 mm. This controlled damage configuration was adopted to systematically investigate the influence of crack depth on the dynamic response and sensing capability of the specimens. Additionally, the location of the damage was also examined in the cementitious specimens in order to assess its influence on the vibration behavior of the specimen, particularly when the damage was positioned at a vibration node or away from it [71,72].

Table 2. Physical and geometrical properties of the detection coil.

No.	Property	Value
1	Coil diameter	57 mm
2	Wire diameter	0.16 mm
3	Threads number	1600
4	Wire material	Copper
5	Electrical resistance	251.7 Ω
6	Coefficient of inductance	0.253 H

3. Results and Discussion

As shown in Figure 4, the recorded response signal of the undamaged cementitious beam specimen was acquired and processed using MATLAB. The upper plot represents the signal in the time domain, where the response amplitude is expressed as voltage (V), while the lower plot represents the corresponding frequency spectrum obtained through FFT analysis.

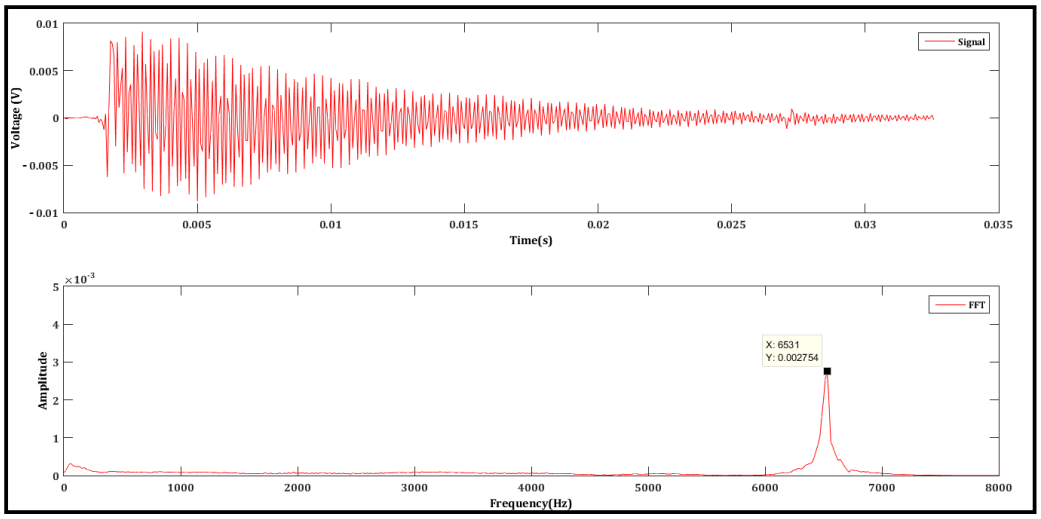


Figure 4. Time- and frequency-domain response of the undamaged cementitious beam specimen.

The FFT amplitude is presented in arbitrary units. It is evident from the time-domain response that the signal exhibits a decaying oscillatory behavior, which is characteristic of a lightly damped structural system after excitation. The response remains stable without irregular fluctuations or sudden discontinuities, suggesting that the specimen maintains consistent dynamic behavior and does not exhibit signs of severe internal defects or damage. The recorded voltage signal originates from the magnetoelastic sensing mechanism of the attached Metglas ribbons. During vibration of the cementitious specimen, alternating mechanical stresses are transferred to the Metglas ribbons, causing continuous changes in their magnetization due to the magnetoelastic effect. These variations generate a time-varying magnetic flux, which is detected by the nearby pickup coil and converted into an electrical voltage signal through electromagnetic induction. Consequently, the measured signal directly reflects the dynamic response characteristics of the specimen. The frequency-domain analysis reveals a dominant resonance peak at 6531 Hz, corresponding to the natural frequency of the undamaged beam specimen. The relatively narrow bandwidth around the resonance peak also suggests low damping and good signal quality. Since natural frequencies are strongly related to structural stiffness, the identified resonance frequency can serve as a reference baseline for comparison with damaged specimens,

where stiffness degradation due to cracking is expected to produce measurable frequency shifts and changes in signal amplitude.

To identify this resonance peak, Euler–Bernoulli beam theory can be applied to the undamaged specimen. According to this theory, for a simply supported beam, the natural bending frequencies are given as follows:

$$f_n = \frac{n^2 \pi}{2L^2} \sqrt{\frac{EI}{\rho A}} \quad (1)$$

where f_n is the n-th natural frequency (Hz), n is the mode number, L is the beam length (m), E is Young's modulus (Pa), I is the second moment of area (m^4), ρ is the material density (kg/m^3), and A is the cross-sectional area (m^2). The cementitious beam specimens considered in this study have a length of L = 0.16 m and a cross-sectional area of A = 0.0016 m^2. The material density, 1886 kg/m^3, was obtained using the vacuum water saturation method. Young's modulus, evaluated from quasi-static stress-strain measurements, was found to be around 22 GPa. Table 3 summarizes the first eight bending modes of the undamaged cementitious specimen, as calculated using Euler–Bernoulli beam theory. By comparing the FFT results with the values reported in the table, a close correspondence is observed with the fourth bending mode, which is likely the dominant mode excited and transmitted through the magnetoelastic sensors. In principle, multiple modes would be expected to be excited and detected. However, this behavior is more clearly observed in metallic materials, where damping effects are significantly lower, allowing a greater number of modes to be identified in the FFT spectrum. In contrast, the cementitious material exhibits stronger damping, which causes the vibration modes to attenuate more rapidly. Consequently, the fourth bending mode dominates the response, while the remaining modes decay faster and are less distinctly captured in the frequency spectrum. Nevertheless, the key conclusion is that the magnetoelastic material used as a vibration sensor is capable of detecting and transmitting the vibration state of the cementitious structure.

Table 3. First eight natural bending frequencies of the undamaged cementitious beam, computed using Euler–Bernoulli beam theory and used for comparison with FFT results.

Mode	Frequency (Hz)
1	387.1
2	1548.6
3	3484.3
4	6194.3
5	9678.7
6	13,937.3
7	18,970.2
8	24,777.4

The fourth bending mode of a simply supported beam, according to Euler–Bernoulli beam theory, is characterized by three internal nodes that are evenly distributed along the beam length. Figure 5 schematically illustrates the location of these nodes. For a 16 cm cementitious beam, the first node is located 4 cm from one end, the second at 8 cm, and the third at 12 cm.

Between the nodes, the bending displacement reaches its maximum amplitude, whereas the displacement at the nodes is theoretically zero. According to the findings of this work [69], it was observed that when damage occurs at locations between the nodes, the corresponding shift in the bending frequency is significant. In contrast, when the damage is located very close to one of the nodes, the frequency shift becomes almost

negligible. This is an important conclusion for vibration-based SHM, because the sensitivity of modal parameters to damage strongly depends on the position of the defect relative to the mode shape. Regions with large modal displacement are considerably more sensitive to stiffness degradation, while nodal regions exhibit limited sensitivity due to the near-zero dynamic response.

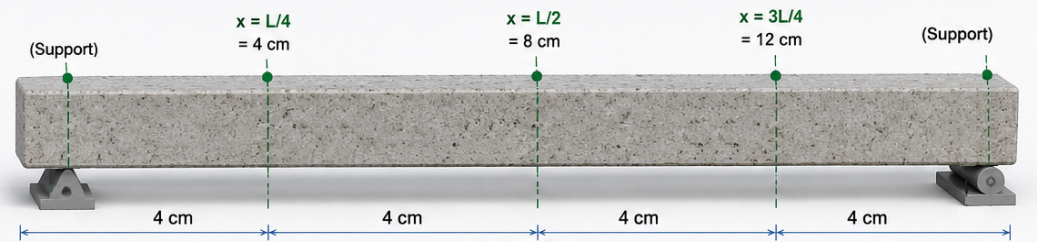


Figure 5. Node locations of the fourth bending mode of a simply supported 16 cm beam.

To test this in practice, the region between the 4 cm and 8 cm nodes was selected as the experimental zone and divided into five damage locations at 4 cm, 5 cm, 6 cm, 7 cm, and 8 cm from the left support. The imposed damage, described previously, consisted of a transverse notch across the specimen's width with a width of 1 mm and a depth of 1 mm. Figure 6 shows the percentage difference in the measured bending mode frequency, defined as the deviation between the undamaged and damaged states, for different damage locations within the region between the 4 cm and 8 cm nodes.

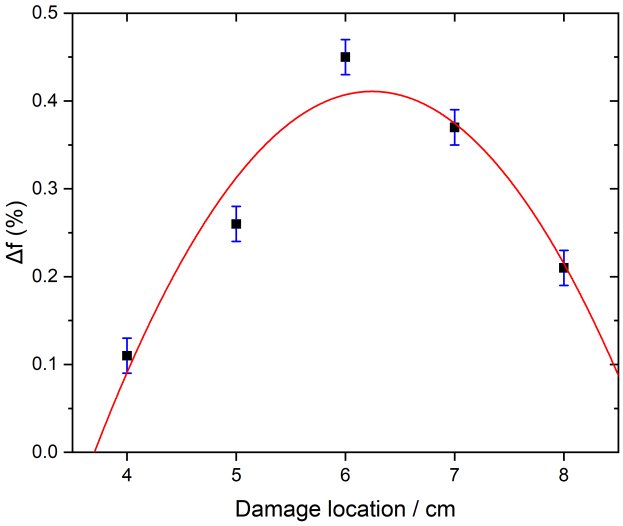
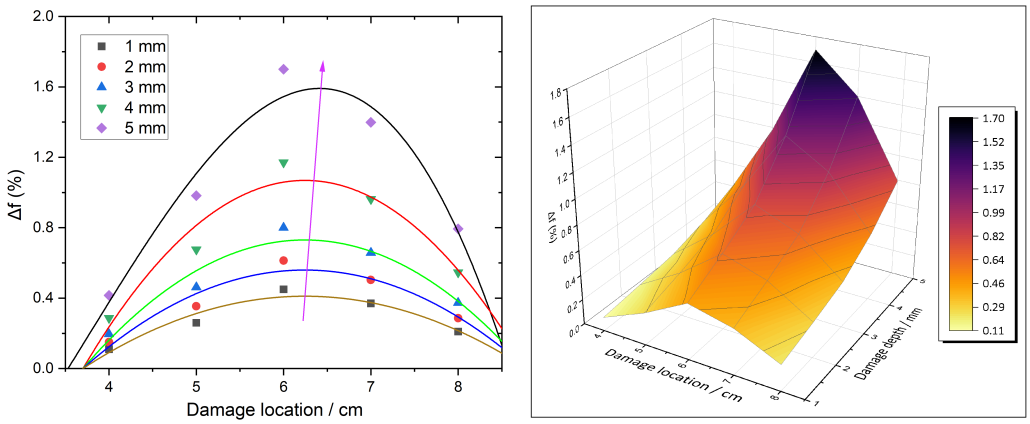


Figure 6. Percentage difference in the fourth bending mode frequency between undamaged and damaged states for various damage locations between the 4 cm and 8 cm nodes.

In this experiment, five cementitious specimens were tested by first measuring their undamaged vibration response, then introducing a fixed damage at a prescribed location, and subsequently repeating the measurements to evaluate the change in dynamic response. As the damage location shifts from the 4 cm node to the 8 cm node, Δf increases sharply and then decreases, reaching a maximum near 6 cm. This supports the earlier statement that the impact of damage on natural frequencies is greater when it is located away from nodal points. Also, from the shape of the plot, we can see that the 8 cm node exhibits a higher value of Δf compared to the 4 cm node, even though both correspond to nodes of the same bending mode. This is most likely attributed to the fact that, in practical experimental conditions, nodal positions are not perfectly invariant due to boundary effects, measurement errors, and asymmetries in the structural condition of the different specimens.

Ideally, the response would show a symmetric dome-shaped profile, with Δf equal to zero at both nodes, reflecting the uniform modal behavior of the mode shape. Nevertheless, the key conclusion remains that the magnetoelastic material used as a vibration sensor is capable of effectively detecting and transmitting both the damage state and the associated nodal behavior, as discussed previously.

Another important parameter investigated was the severity of the damage, which was experimentally simulated by increasing the depth of the notch-shaped crack. The crack depth was varied from 1 mm to 5 mm, and the same specimens used in the crack location experiment were employed here, meaning that the crack depth variation was also evaluated across all five previously defined damage locations. Figure 7 collectively illustrate a consistent, non-linear relationship between structural damage parameters and the measured frequency shift Δf.



(**a**) (**b**)

Figure 7. Effect of damage location and depth on frequency shift Δf: (**a**) location-dependent response for different crack depths, and (**b**) 3D surface showing their combined influence.

In Figure 7a, the curves shown were obtained by fitting a second-degree polynomial to the measured data. The selection of the second-order fit was based on a comparative analysis of fitting performance across first-, second-, and third-order polynomial models. The average adjusted R-squared value across all datasets was 0.2882 for the first-order fit, 0.8482 for the second-order fit, and 0.8379 for the third-order fit. Although the second- and third-order models demonstrated similar performance, the second-order polynomial was selected for all datasets due to its slightly superior average adjusted R-squared value. It can be observed that, as the depth of the notch-shaped crack increases, the corresponding frequency shift also increases for every damage location, indicating a monotonic relationship while preserving the overall parabolic profile. Additionally, as indicated by the arrow, the maximum values of each fitted parabola exhibit a positional shift. Although the maximum shift theoretically occurs symmetrically between the nodes, the fitting analysis reveals that this location gradually shifts in practice as the severity of the damage increases. Complementing this, the 3D surface map in Figure 7b provides a comprehensive visualization of these trends, highlighting a synergistic effect where the maximum frequency shift occurs at the confluence of the deepest damage of 5 mm and the most sensitive location of 6 cm. Based on these results, it should be emphasized once again that the expected vibrational behavior of the cementitious material specimens is accurately captured by the magnetoelastic sensor. This demonstrates the high sensitivity of the sensor and its capability to effectively detect and magnetically transmit the measured signal from the category of materials.

4. Conclusions

In the present study, the vibration behavior of cementitious beam specimens was experimentally investigated using magnetoelastic sensing technology under both undamaged and damaged conditions. The attached Metglas ribbons successfully captured the dynamic response of the specimens through the magnetoelastic effect, while the induced magnetic flux variations were effectively converted into measurable electrical signals using a pickup coil.

The experimental results showed that the dominant resonance frequency identified through FFT analysis corresponded closely to the fourth bending mode predicted by Euler–Bernoulli beam theory. This agreement confirms the capability of the magnetoelastic sensing approach to reliably monitor the vibrational characteristics of cementitious materials. Although multiple vibration modes are theoretically expected, the relatively high damping properties of cementitious materials caused other modes to attenuate rapidly, resulting in the fourth bending mode dominating the recorded response.

The influence of damage location on the vibration response demonstrated that the sensitivity of the frequency shift strongly depends on the position of the crack relative to the modal shape. Damage introduced near nodal regions produced minimal frequency variation, whereas damage located between the nodes generated significantly larger shifts, with the maximum response observed near the center of the modal displacement region. These findings validate the theoretical expectation that vibration-based damage sensitivity is maximized in regions of high modal displacement.

In addition, the investigation of crack depth revealed a monotonic increase in frequency shift with increasing damage severity for all tested locations. The fitted polynomial curves and 3D surface representation confirmed a non-linear interaction between damage depth and location, while also indicating a gradual shift in the position of maximum sensitivity as the crack severity increased. This behavior highlights the complex influence of stiffness degradation on the modal response of cementitious structures.

Overall, the study demonstrates that magnetoelastic materials can act as highly sensitive and reliable passive sensors for vibration-based structural health monitoring of cementitious structures. The proposed sensing methodology successfully captures changes in the dynamic response associated with both damage location and severity, while simultaneously enabling magnetic transmission of the information without direct electrical contact. These results highlight the strong potential of magnetoelastic sensing systems for future structural health monitoring applications in civil engineering materials and infrastructure systems.

Funding: This research received no external funding.

Data Availability Statement: Data are available on request from the author.

Acknowledgments: The author would like to express sincere gratitude to Dimitris Kouzoudis in the Department of Chemical Engineering at the University of Patras, Greece, for his valuable discussions and insightful suggestions, which significantly contributed to this work. During the preparation of this work, the author used AI tools, including GPT-5.3-mini model and Gemini, to improve the readability and quality of the language, as well as the schematic graphics. After using these tools, the author thoroughly reviewed and revised the content as needed and accepts full responsibility for the final version of the publication.

Conflicts of Interest: The author declares no conflicts of interest.

References

1. Speckmann, H.; Henrich, R. Structural health monitoring (SHM)–overview on technologies under development. In Proceedings of the 16th World Conference on NDT, Montreal, QC, Canada, 30 August–3 September 2004; Volume 1.

2. Warsi, Z.H.; Irshad, S.M.; Khan, F.; Shahbaz, M.A.; Junaid, M.; Amin, S.U. Sensors for structural health monitoring: A review. In *2019 Second International Conference on Latest trends in Electrical Engineering and Computing Technologies (INTELLECT)*; IEEE: New York, NY, USA, 2019; pp. 1–6.
3. Maraveas, C.; Bartzanas, T. Sensors for structural health monitoring of agricultural structures. *Sensors* **2021**, *21*, 314. [CrossRef]
4. Rocha, H.; Semprimoschnig, C.; Nunes, J.P. Sensors for process and structural health monitoring of aerospace composites: A review. *Eng. Struct.* **2021**, *237*, 112231. [CrossRef]
5. Kang, I.; Schulz, M.J.; Kim, J.H.; Shanov, V.; Shi, D. A carbon nanotube strain sensor for structural health monitoring. *Smart Mater. Struct.* **2006**, *15*, 737–748. [CrossRef]
6. Liu, Z.; Mrad, N. Validation of strain gauges for structural health monitoring with Bayesian belief networks. *IEEE Sens. J.* **2012**, *13*, 400–407. [CrossRef]
7. Dos Reis, J.; Oliveira Costa, C.; Sá da Costa, J. Strain gauges debonding fault detection for structural health monitoring. *Struct. Control Health Monit.* **2018**, *25*, e2264. [CrossRef]
8. Xiao, T.; Qian, C.; Yin, R.; Wang, K.; Gao, Y.; Xuan, F. 3D printing of flexible strain sensor array based on UV-curable multiwalled carbon nanotube/elastomer composite. *Adv. Mater. Technol.* **2021**, *6*, 2000745.
9. Qiang, Y.; Chen, Z.; Yang, L.; Huang, Q.; Li, D.; Huang, W.; Guo, X.; Zhang, C. Ultrafast self-powered strain sensor utilizing a flexible solar cell. *Nano Energy* **2025**, *139*, 110920. [CrossRef]
10. Song, G.; Gu, H.; Li, H. Application of the piezoelectric materials for health monitoring in civil engineering: An overview. In *Engineering, Construction, and Operations in Challenging Environments: Earth and Space 2004*; American Society of Civil Engineers (ASCE): Orlando, FL, USA, 2004; pp. 680–687.
11. Yan, S.; Wu, J.; Sun, W.; Ma, H.; Yan, H. Development and application of structural health monitoring system based on piezoelectric sensors. *Int. J. Distrib. Sens. Netw.* **2013**, *9*, 270927. [CrossRef]
12. Song, S.; Hou, Y.; Guo, M.; Wang, L.; Tong, X.; Wu, J. An investigation on the aggregate-shape embedded piezoelectric sensor for civil infrastructure health monitoring. *Constr. Build. Mater.* **2017**, *131*, 57–65. [CrossRef]
13. Ghosh, A.; Edwards, D.J.; Hosseini, M.R.; Al-Ameri, R.; Abawajy, J.; Thwala, W.D. Real-time structural health monitoring for concrete beams: A cost-effective 'Industry 4.0'solution using piezo sensors. *Int. J. Build. Pathol. Adapt.* **2021**, *39*, 283–311.
14. Julphunthong, P.; Wiwatrojanagul, P.; Tiantong, P.; Bongkarn, T.; Rianyoi, R.; Potong, R. Development and evaluation of KNLNTS-cement composites for use as piezoelectric sensors in structural health monitoring applications. *Results Eng.* **2025**, *25*, 104526. [CrossRef]
15. Tennyson, R.; Mufti, A.; Rizkalla, S.; Tadros, G.; Benmokrane, B. Structural health monitoring of innovative bridges in Canada with fiber optic sensors. *Smart Mater. Struct.* **2001**, *10*, 560–573. [CrossRef]
16. Inaudi, D.; Glisic, B. Overview of fibre optic sensing applications to structural health monitoring. In *Symposium on Deformation Measurement and Analysis*; FIG (International Federation of Surveyors): Lisbon, Portugal, 2008; pp. 1–10.
17. Sigurdardottir, D.; Glisic, B. On-site validation of fiber-optic methods for structural health monitoring: Streicker Bridge. *J. Civ. Struct. Health Monit.* **2015**, *5*, 529–549.
18. Wu, T.; Liu, G.; Fu, S.; Xing, F. Recent progress of fiber-optic sensors for the structural health monitoring of civil infrastructure. *Sensors* **2020**, *20*, 4517. [CrossRef] [PubMed]
19. Farahbakhsh, S.; Chamoin, L.; Poncelet, M. Continuous structural health monitoring with a modified dual Kalman filter applied with optical fiber sensing data. *Comput. Struct.* **2026**, *329*, 108284. [CrossRef]
20. Lynch, J.P.; Partridge, A.; Law, K.H.; Kenny, T.W.; Kiremidjian, A.S.; Carryer, E. Design of piezoresistive MEMS-based accelerometer for integration with wireless sensing unit for structural monitoring. *J. Aerosp. Eng.* **2003**, *16*, 108–114. [CrossRef]
21. Jo, H.; Rice, J.A.; Spencer, B.F., Jr.; Nagayama, T. Development of high-sensitivity accelerometer board for structural health monitoring. In *Sensors and Smart Structures Technologies for Civil, Mechanical, and Aerospace Systems 2010*; SPIE: Bellingham, WA, USA, 2010; Volume 7647, pp. 39–50.
22. Bowe, C.; Quirke, P.; Cantero, D.; O'Brien, E.J. Drive-by structural health monitoring of railway bridges using train mounted accelerometers. In *5th ECCOMAS Thematic Conference on Computational Methods in Structural Dynamics and Earthquake Engineering 2015*; Papadrakasis, M., Papadopoulos, V., Plevris, V., Eds.; NTUA (National Technical University of Athens): Athens, Greece, 2015.
23. Shen, N.; Chen, L.; Chen, R. Multi-route fusion method of GNSS and accelerometer for structural health monitoring. *J. Ind. Inf. Integr.* **2023**, *32*, 100442. [CrossRef]
24. Occhipinti, G.; Lo Iacono, F.; Tusa, G.; Costanza, A.; Fertitta, G.; Lodato, L.; Macaluso, F.; Martino, C.; Mugnos, G.; Oliva, M.; et al. Shake Table Tests on Scaled Masonry Building: Comparison of Performance of Various Micro-Electromechanical System Accelerometers (MEMS) for Structural Health Monitoring. *Sensors* **2025**, *25*, 1010. [CrossRef] [PubMed]
25. Finlayson, R.D.; Friesel, M.A.; Carlos, M.F.; Miller, R.K.; Godinez, V. Acoustic emission structural health management systems (AE-SHMS). In *Nondestructive Evaluation of Aging Aircraft, Airports, and Aerospace Hardware IV*; SPIE: Bellingham, WA, USA, 2000; Volume 3994, pp. 128–137.

26. Tan, A.C.; Kaphle, M.; Thambiratnam, D. Structural health monitoring of bridges using acoustic emission technology. In *2009 8th International Conference on Reliability, Maintainability and Safety*; IEEE: New York, NY, USA, 2009; pp. 839–843.
27. Khan, M.T.I.; Tawhidul, I. Structural health monitoring by acoustic emission. In *Structural Health Monitoring from Sensing to Processing*; IntechOpen: London, UK, 2018; Volume 23.
28. Cui, J.; Qu, X.; Lv, C.; Du, J.; Wang, H. Multi-parameter acoustic emission analysis for fatigue crack evaluation in structural health monitoring. *Measurement* **2025**, *256*, 118529. [CrossRef]
29. Wang, J.F.; Lin, K.X.; Lin, J.F.; Zhou, H.J. A review on acoustic emission-based damage detection and quantitative assessment of civil engineering structures in recent years. *Struct. Health Monit.* **2026**. [CrossRef]
30. Staszewski, W.J.; Lee, B.; Mallet, L.; Scarpa, F. Structural health monitoring using scanning laser vibrometry: I. Lamb wave sensing. *Smart Mater. Struct.* **2004**, *13*, 251–260. [CrossRef]
31. Moll, J.; Bechtel, K.; Hils, B.; Krozer, V. Mechanical vibration sensing for structural health monitoring using a millimeter-wave doppler radar sensor. In Proceedings of the EWSHM-7th European Workshop on Structural Health Monitoring, Nantes, France, 8–11 July 2014.
32. Klun, M.; Zupan, D.; Lopatič, J.; Kryžanowski, A. On the application of laser vibrometry to perform structural health monitoring in non-stationary conditions of a hydropower dam. *Sensors* **2019**, *19*, 3811. [CrossRef] [PubMed]
33. Markov, V.; Kupiec, S.; Weldon, J.; Abejar, J.; Erwin, D. Laser Doppler imaging vibrometer for real-time health monitoring of civil infrastructures. In *Nondestructive Characterization and Monitoring of Advanced Materials, Aerospace, Civil Infrastructure, and Transportation XVI*; SPIE: Bellingham, WA, USA, 2022; Volume 12047, pp. 293–302.
34. Fu, L.; Ahmed, Z.; Kim, D.; Seo, H. Monitoring dynamic behavior of bridges through wavelet transform of laser doppler vibrometer signal. *J. Civ. Struct. Health Monit.* **2025**, *15*, 1639–1654. [CrossRef]
35. Lynch, J.P.; Loh, K.J. A summary review of wireless sensors and sensor networks for structural health monitoring. *Shock Vib. Dig.* **2006**, *38*, 91–130. [CrossRef]
36. Noel, A.B.; Abdaoui, A.; Elfouly, T.; Ahmed, M.H.; Badawy, A.; Shehata, M.S. Structural health monitoring using wireless sensor networks: A comprehensive survey. *IEEE Commun. Surv. Tutor.* **2017**, *19*, 1403–1423. [CrossRef]
37. Veluthedath Shajihan, S.A.; Chow, R.; Mechitov, K.; Fu, Y.; Hoang, T.; Spencer, B.F., Jr. Development of synchronized high-sensitivity wireless accelerometer for structural health monitoring. *Sensors* **2020**, *20*, 4169. [CrossRef] [PubMed]
38. Ali, Z.; Shah, A. Structural health monitoring using wireless sensor networks. *J. Adv. Electr. Electron. Eng.* **2025**, *1*, 34–41.
39. Wang, M.; Koo, K.Y.; Xu, F.; Brownjohn, J. A Wirelessly Time-Synchronized Vision-Based System Network for Non-Contact Structural Health Monitoring. In *Computer Vision & Laser Vibrometry*; River Publishers: Gistrup, Denmark, 2026; Volume 6, pp. 23–30.
40. Yuan, F.G.; Zargar, S.A.; Chen, Q.; Wang, S. Machine learning for structural health monitoring: Challenges and opportunities. In *Sensors and Smart Structures Technologies for Civil, Mechanical, and Aerospace Systems 2020*; SPIE: Bellingham, WA, USA, 2020; Volume 11379, p. 1137903.
41. Zinno, R.; Haghshenas, S.S.; Guido, G.; VItale, A. Artificial intelligence and structural health monitoring of bridges: A review of the state-of-the-art. *IEEE Access* **2022**, *10*, 88058–88078. [CrossRef]
42. Sun, Y.; Liu, S.; Li, R.; Ye, Z.; Kang, Y.; Chen, S. A new magnetic flux leakage sensor based on open magnetizing method and its on-line automated structural health monitoring methodology. *Struct. Health Monit.* **2015**, *14*, 583–603. [CrossRef]
43. Davis, A.; Mirsayar, M.; Hartl, D. A novel structural health monitoring approach in concrete structures using embedded magnetic shape memory alloy components. *Constr. Build. Mater.* **2021**, *311*, 125212. [CrossRef]
44. Amorim, L.; Martins, P.; Tubio, C.R.; Seoane-Rivero, R.; Lanceros-Mendez, S. Magnetic Field-Based Strategy for Damage Detection and Stratigraphy Assessment for Structural Health Monitoring Applications. *Adv. Eng. Mater.* **2025**, *27*, e202501217.
45. Elyasigorji, A.; Rezaee, M.; Ghorbanpoor, A. Magnetic corrosion detection in concrete structures. In *International Conference on Sustainable Infrastructure 2019*; American Society of Civil Engineers: Reston, VA, USA, 2019; pp. 175–184.
46. Weng, G.; Wang, J.; Liu, Y.; Zhu, X.; Dai, J. Magnetic stress sensing system for nondestructive stress testing of structural steel and steel truss components based on existing magnetism. *Sensors* **2020**, *20*, 4043. [CrossRef] [PubMed]
47. Tapeinos, C.I.; Kouzoudis, D.; Varvatsoulis, K.; Vázquez, M.; Samourgkanidis, G. Microwire vs. Micro-Ribbon Magnetoelastic Sensors for Vibration-Based Structural Health Monitoring of Rectangular Concrete Beams. *Sensors* **2025**, *25*, 3590. [PubMed]
48. Samourgkanidis, G.; Nikolaou, P.; Gkovosdis-Louvaris, A.; Sakellis, E.; Blana, I.M.; Topoglidis, E. Hemin-modified SnO2/metglas electrodes for the simultaneous electrochemical and magnetoelastic sensing of H2O2. *Coatings* **2018**, *8*, 284.
49. Kouzoudis, D.; Baimpos, T.; Samourgkanidis, G. A new method for the measurement of the diffusion coefficient of adsorbed vapors in thin zeolite films, based on magnetoelastic sensors. *Sensors* **2020**, *20*, 3251. [CrossRef] [PubMed]
50. Samourgkanidis, G.; Kouzoudis, D. Characterization of magnetoelastic ribbons as vibration sensors based on the measured natural frequencies of a cantilever beam. *Sens. Actuators A Phys.* **2020**, *301*, 111711. [CrossRef]
51. Samourgkanidis, G.; Kouzoudis, D. Magnetoelastic ribbons as vibration sensors for real-time health monitoring of rotating metal beams. *Sensors* **2021**, *21*, 8122. [CrossRef] [PubMed]

52. Das, S.; Saha, P.; Patro, S.K. Vibration-based damage detection techniques used for health monitoring of structures: A review. *J. Civ. Struct. Health Monit.* **2016**, *6*, 477–507. [CrossRef]
53. Zar, A.; Hussain, Z.; Akbar, M.; Rabczuk, T.; Lin, Z.; Li, S.; Ahmed, B. Towards vibration-based damage detection of civil engineering structures: Overview, challenges, and future prospects. *Int. J. Mech. Mater. Des.* **2024**, *20*, 591–662. [CrossRef]
54. De Maio, U.; Garro, A.; Greco, F.; Pranno, A.; Silvestri, A. Vibration-based damage identification in concrete beams via a decomposed deep learning approach. *Prog. Eng. Sci.* **2026**, *3*, 100280. [CrossRef]
55. He, K.; Zhu, W. Structural damage detection using changes in natural frequencies: Theory and applications. *J. Phys. Conf. Ser.* **2011**, *305*, 012054. [CrossRef]
56. Sha, G.; Radzieński, M.; Cao, M.; Ostachowicz, W. A novel method for single and multiple damage detection in beams using relative natural frequency changes. *Mech. Syst. Signal Process.* **2019**, *132*, 335–352. [CrossRef]
57. Dubey, A.; Denis, V.; Serra, R. Sensitivity and efficiency of the frequency shift coefficient based on the damage identification algorithm: Modeling uncertainty on natural frequencies. *Vibration* **2022**, *5*, 59–79. [CrossRef]
58. Rucevskis, S.; Wesolowski, M. Identification of damage in a beam structure by using mode shape curvature squares. *Shock Vib.* **2010**, *17*, 601–610. [CrossRef]
59. Rucevskis, S.; Janeliukstis, R.; Akishin, P.; Chate, A. Mode shape-based damage detection in plate structure without baseline data. *Struct. Control Health Monit.* **2016**, *23*, 1180–1193. [CrossRef]
60. Huang, M.; Xu, Z.; Cai, C.; Chen, D.; Yin, W.; He, X. Vibration-based damage detection in laminated composite plates: A novel approach using superposition of higher-order derivatives of mode shapes. *Struct. Health Monit.* **2025**. [CrossRef]
61. Frizzarin, M.; Feng, M.Q.; Franchetti, P.; Soyoz, S.; Modena, C. Damage detection based on damping analysis of ambient vibration data. *Struct. Control Health Monit. Off. J. Int. Assoc. Struct. Control Monit. Eur. Assoc. Control Struct.* **2010**, *17*, 368–385.
62. Cao, M.; Sha, G.; Gao, Y.F.; Ostachowicz, W. Structural damage identification using damping: A compendium of uses and features. *Smart Mater. Struct.* **2017**, *26*, 043001. [CrossRef]
63. Gohar, S.; Matsumoto, Y.; Maki, T.; Sakuma, S. Investigation into vibration-based structural damage identification and amplitude-dependent damping ratio of reinforced concrete bridge deck slab under different loading states. *J. Civ. Struct. Health Monit.* **2023**, *13*, 133–148.
64. Kouzoudis, D.; Samourgkanidis, G.; Tapeinos, C.I. Contactless Detection of Natural Bending Frequencies using Embedded Metallic-Glass Ribbons inside Plastic Beams made of 3-D Printing. *Recent Prog. Mater.* **2021**, *3*, 1. [CrossRef]
65. *EN 196-1:2016*; Methods of Testing Cement—Part 1: Determination of Strength. European Committee for Standardization (CEN): Brussels, Belgium, 2016.
66. *EN 1015-3:1999*; Methods of Test for Mortar for Masonry—Part 3: Determination of Consistence of Fresh Mortar (by Flow Table). European Committee for Standardization (CEN): Brussels, Belgium, 1999.
67. Samourgkanidis, G.; Varvatsoulis, K.; Kouzoudis, D. The Effect of the Thermal Annealing Process to the Sensing Performance of Magnetoelastic Ribbon Materials. *Sustainability* **2021**, *13*, 13947. [CrossRef]
68. Samourgkanidis, G.; Kouzoudis, D.; Charalampous, P.; Adnan, E. Signal Enhancement in Magnetoelastic Ribbons Through Thermal Annealing: Evaluation of Magnetic Signal Output in Different Metglas Materials. *Sensors* **2025**, *25*, 3722. [CrossRef] [PubMed]
69. Samourgkanidis, G.; Kouzoudis, D. Experimental detection by magnetoelastic sensors and computational analysis with finite elements, of the bending modes of a cantilever beam with minor damage. *Sens. Actuators A Phys.* **2018**, *276*, 155–164. [CrossRef]
70. Tapeinos, C.I.; Kamitsou, M.D.; Dassios, K.G.; Kouzoudis, D.; Christogerou, A.; Samourgkanidis, G. Contactless and Vibration-Based Damage Detection in Rectangular Cement Beams Using Magnetoelastic Ribbon Sensors. *Sensors* **2023**, *23*, 5453. [CrossRef] [PubMed]
71. Morassi, A.; Rocchetto, L. A damage analysis of steel-concrete composite beams via dynamic methods: Part I. Experimental results. *J. Vib. Control* **2003**, *9*, 507–527. [CrossRef]
72. Samourgkanidis, G.; Kouzoudis, D. A pattern matching identification method of cracks on cantilever beams through their bending modes measured by magnetoelastic sensors. *Theor. Appl. Fract. Mech.* **2019**, *103*, 102266. [CrossRef]

Disclaimer/Publisher's Note: The statements, opinions and data contained in all publications are solely those of the individual author(s) and contributor(s) and not of MDPI and/or the editor(s). MDPI and/or the editor(s) disclaim responsibility for any injury to people or property resulting from any ideas, methods, instructions or products referred to in the content.